Molecular Biology of the Cell
Vol. 11, 3177–3190, September 2000

Neuronal Cell Shape and Neurite Initiation Are Regulated by the Ndr Kinase SAX-1, a Member of the Orb6/COT-1/Warts Serine/Threonine Kinase Family

Jennifer A. Zallen,* Erin L. Peckol†, David M. Tobin, and Cornelia I. Bargmann*‡

Howard Hughes Medical Institute, Programs in Developmental Biology, Neuroscience, and Genetics, Department of Anatomy and Department of Biochemistry and Biophysics, The University of California, San Francisco, California 94143

Submitted April 5, 2000; Revised June 9, 2000; Accepted July 5, 2000
Monitoring Editor: Judith Kimble

The *Caenorhabditis elegans sax-1* gene regulates several aspects of neuronal cell shape. *sax-1* mutants have expanded cell bodies and ectopic neurites in many classes of neurons, suggesting that SAX-1 functions to restrict cell and neurite growth. The ectopic neurites in sensory neurons of *sax-1* mutants resemble the defects caused by decreased sensory activity. However, the activity-dependent pathway, mediated in part by the UNC-43 calcium/calmodulin-dependent kinase II, functions in parallel with SAX-1 to suppress neurite initiation. *sax-1* encodes a serine/threonine kinase in the Ndr family that is related to the Orb6 (*Schizosaccharomyces pombe*), Warts/Lats (*Drosophila*), and COT-1 (*Neurospora*) kinases that function in cell shape regulation. These kinases have similarity to Rho kinases but lack consensus Rho-binding domains. Dominant negative mutations in the *C. elegans* RhoA GTPase cause neuronal cell shape defects similar to those of *sax-1* mutants, and genetic interactions between *rhoA* and *sax-1* suggest shared functions. These results suggest that SAX-1/Ndr kinases are endogenous inhibitors of neurite initiation and cell spreading.

INTRODUCTION

Neuronal cells have complex morphologies, with distinctive cell bodies, axons, and dendrites. Although extrinsic cues that regulate axon guidance and branching have been defined (Tessier-Lavigne and Goodman, 1996; Mueller, 1999; Wang *et al.*, 1999), less is known about the intrinsic determinants of cell shape. The mechanisms that determine a neuron's competence to form neurites, the number of neurites per cell, and the subcellular site of neurite initiation are unknown.

Rho family GTPases affect the actin cytoskeleton and morphology of many cell types (Hall, 1994). These GTPases exert their activity by binding and regulating multiple targets, including actin-binding proteins and several classes of kinases (Tapon and Hall, 1997). The Rho family GTPases Rac and Cdc42 are implicated in cell motility and axon outgrowth (Ridley *et al.*, 1992; Luo *et al.*, 1994; Kozma *et al.*, 1995; Nobes and Hall, 1995; Luo *et al.*, 1997), and Rho is implicated in contractile events such as stress fiber formation and neurite retraction (Paterson *et al.*, 1990; Ridley and Hall, 1992; Jalink *et al.*, 1994; Gebbink *et al.*, 1997). Rho acts in part through the Rho kinase family, which includes Rho kinase (Leung *et al.*, 1995; Ishizaki *et al.*, 1996; Matsui *et al.*, 1996), LET-502 (Wissmann *et al.*, 1997), Genghis Khan (Luo *et al.*, 1997), Citron (Di Cunto *et al.*, 1998; Madaule *et al.*, 1998), and MRCK (Leung *et al.*, 1998). These proteins share a related kinase catalytic domain as well as domains that allow GTPase association. Mutations in the *Caenorhabditis elegans* LET-502 kinase prevent the epidermal cell shape changes that drive embryonic elongation, whereas mutations in Genghis Khan disrupt actin structures in the *Drosophila* egg chamber (Luo *et al.*, 1997; Wissmann *et al.*, 1997). These phenotypes, together with functional studies in cultured cells (Leung *et al.*, 1996; Amano *et al.*, 1997; Ishizaki *et al.*, 1997), implicate Rho kinases in the regulation of cell morphology.

Members of a distinct family of serine/threonine kinases, including Orb6, COT-1, and Warts/Lats, are required for the regulation of cell morphology and cell division (Yarden *et al.*, 1992; Justice *et al.*, 1995; Xu *et al.*, 1995; Verde *et al.*, 1998). Kinases in the Orb6/COT-1/Warts family are closely related to Rho kinases in the kinase catalytic domain but lack consensus Rho-binding motifs. The pathways that regulate these kinases are not fully defined. Orb6 functions downstream of Pak1/Shk1 kinase (Verde *et al.*, 1998), which acts together with the Cdc42 GTPase in cell shape regulation (Marcus *et al.*, 1995; Ottilie *et al.*, 1995). An expressed se-

Present addresses: * Department of Molecular Biology, Princeton University, Princeton, NJ 08544; and † Project BIOTECH, University of Arizona, Tucson, AZ 85721.
‡ Corresponding author. E-mail address: cori@itsa.ucsf.edu.

quence tag (EST) in *C. elegans* led to the identification of Ndr, a new member of the Orb6/COT-1/Warts kinase family that is conserved in *C. elegans*, *Drosophila*, and humans (Millward *et al.*, 1995). The function of the Ndr kinases is not known.

A screen for mutants with altered neuronal morphology in *C. elegans* identified mutations in the *sax-1* and *sax-2* genes (Zallen *et al.*, 1999). Here we show that *sax-1* encodes the *C. elegans* Ndr kinase, a member of the Orb6/COT-1/Warts family. *sax-1* and *sax-2* mutants exhibit defects in neuronal cell shape and polarity: cells appear expanded and irregular instead of compact and spherical, and they initiate ectopic neurites in addition to the normal axon and dendrite. Similar cell shape defects are caused by dominant negative mutations in the *C. elegans* RhoA GTPase. In sensory neurons, ectopic neurites are also caused by mutations that disrupt neuronal activity (Coburn and Bargmann, 1996; Coburn *et al.*, 1998; Peckol *et al.*, 1999). We find that the activity-dependent pathway for neurite initiation is modulated by the UNC-43 calcium/calmodulin-dependent protein kinase II (CaMKII) and functions in parallel with the SAX-1 (GenBank accession number AF275634) kinase to regulate neurite initiation.

MATERIALS AND METHODS

Strains and Genetics

Wild-type animals were *C. elegans* variety Bristol, strain N2. Strains were maintained at 20 or 25°C by standard methods (Brenner, 1974). Some strains were provided by the *Caenorhabditis* Genetics Center (St. Paul, MN).

sax-1 and *sax-2* mutant alleles (Zallen *et al.*, 1999) were outcrossed twice by *kyIs4* X; *him-5(e1490)* V, once by *kyIs4* X, and once by N2. Sensory axon defects detected by the *ceh-23::gfp kyIs4* transgene were followed to map *sax-1(ky211)* to LGX. Five of five *lon-2* non–*lin-18 unc-78* recombinants and two of four *lon-2 lin-18* non–*unc-78* recombinants were mutant for *sax-1*. Two of seven *lon-2* non–*fax-1* recombinants were mutant for *sax-1*.

The *stP40* restriction fragment length polymorphism that differs between the Bristol strains RW7000 and N2 was used to further map *sax-1*. Recombinants were isolated from *unc-20(e112ts) sax-1(ky211) lon-2(e648)*/RW7000 heterozygotes. None of three *unc-20 sax-1* non–*lon-2* recombinants and two of two *unc-20* non–*sax-1 lon-2* recombinants segregated the RW7000 *stP40* polymorphism. None of two *lon-2 sax-1* non–*unc-20* recombinants and three of three *lon-2* non–*sax-1 unc-20* recombinants segregated the *stP40* polymorphism. These mapping data placed *sax-1* to the left of *lin-18* and to the right or close on the left of *stP40* on LGX.

Germline Transformation

Transgenic strains were created as described (Mello *et al.*, 1991). Multiple lines from each injection were characterized for rescue of the sensory axon defects in the *sax-1(ky211) kyIs4* X strain. Cosmids spanning the region between *stP40* and *lin-18* were injected at 10 ng/μl each in pools of four to five cosmids with the use of the dominant pRF4 *rol-6(su1006)* plasmid at 100 ng/μl as a coinjection marker. Cosmids from the rescuing pool were injected individually at 30 ng/μl with pRF4. Rescue activity of the R11G1 cosmid was retained in a 17-kilobase (kb) *Sac*II–*Nar*I subclone of the R11G1 cosmid cloned into the *Sac*II–*Cla*I sites of pBSKII (pJAZ19, injected at 30 ng/μl) and a 7.7-kb *Sac*II–*Xho*I subclone of the R11G1 cosmid cloned into the *Sac*II–*Xho*I sites of pBSKII (pJAZ29, injected at 50 ng/μl). A deletion in the pJAZ19 *sax-1* rescuing construct was made by digestion with *Bal*I and religation, removing 1 kb of genomic sequence that deletes conserved kinase domains V (part), VIa, VIb, and VII (part) and breaks within an intron, which is predicted to disrupt *sax-1* splicing. This deletion construct (pJAZ30) was injected at 30 ng/μl with pRF4.

cDNA Isolation and Allele Sequencing

A high-stringency screen of 5×10^5 plaques of a mixed-stage *C. elegans* cDNA library (Barstead and Waterston, 1989) that used the cm11b8 cDNA as a probe (a generous gift from R. Waterston, Washington University, St. Louis, MO) identified 15 full-length *sax-1* cDNAs and 1 partial cDNA. Six cDNAs were fully sequenced and the rest were partially sequenced, encoding a predicted protein of 467 or 469 amino acids. The *sax-1* sequence was confirmed, and its genomic organization was determined by aligning the cDNA with reported genomic sequences from the *C. elegans* Sequencing Consortium (1998); however, it differs from the gene predicted in that region (see below). The cDNAs were flanked by a 38-base pair 5′ untranslated region (UTR), a 335-base pair 3′ UTR, and a poly(A) tail.

The *sax-1(ky211)* mutation was identified by sequencing the *sax-1* ORF and splice junctions from genomic DNA amplified with the use of the Expand PCR kit (Boehringer Mannheim, Indianapolis, IN). PCR fragments were sequenced on one strand with the use of the *fmol* sequencing kit (Promega, Madison, WI). The mutation was confirmed by sequencing a separately amplified PCR fragment.

The *C. elegans* Sequencing Consortium (1998) predicted a longer 1356-amino acid protein in the *sax-1* region, including *sax-1* exons and additional downstream exons. To determine whether these downstream exons could encode alternative exons of *sax-1*, we sequenced five ESTs kindly provided by Y. Kohara (National Institute of Genetics, Mishima, Japan); the longest contained 712 amino acids in addition to the 3′ UTR. The 5′ end of this transcript was identified by reverse transcription (RT)-PCR from wild-type N2 RNA prepared by Trizol extraction (GIBCO-BRL, Gaithersburg, MD) with the use of 3′ primers from the predicted ESTs in combination with a 5′ primer to the *C. elegans* SL2 spliced leader sequence. The SL2 spliced leader sequence is present at the 5′ end of *C. elegans* genes that are located downstream in an operon (Zorio *et al.*, 1994). The full-length transcript encodes a predicted 811-amino acid protein. We named this transcript *stg-1*, for *sax-1* three-prime gene. The *stg-1* coding region was not required for *sax-1* rescue. No transcripts were identified that extended from the *stg-1* coding region into the *sax-1* coding region or the SL1 spliced leader sequence. An additional in-frame *stg-1* exon upstream of the SL2 splice junction was present in one of the five cDNAs; however, the 5′ end of this transcript was not detected by RT-PCR. Therefore, *sax-1* and *stg-1* appear to encode distinct protein products that may belong to a common operon, although it is possible that they are also included in a single transcript that was not detected by ESTs or RT-PCR.

Characterization of Neuronal Morphology

Axons were scored in living adult animals, except for larval animals scored in Figure 2. The AWC neurons were visualized with an integrated *str-2::gfp* transgene (*kyIs140 I*; Dwyer *et al.*, 1998). The ASER neuron was visualized with an integrated *gcy-5::gfp* transgene (*kyIs164 II*; Yu *et al.*, 1997). The ASJ neurons shown in Figures 1 and 2 and described in Table 1 were visualized with an integrated *tax-2*Δ*::gfp* transgene (*kyIs150 IV*; Coburn and Bargmann, 1996; Peckol *et al.*, 1999). *tax-2*Δ*::gfp* labels ASJ along with the AWB, AWC, ASG, ASI, and ASK amphid chemosensory neuron pairs. Transgenes were integrated by trimethylpsoralen and UV radiation and outcrossed three to seven times. In Figures 3 and 5, ASJ neurons were visualized in the absence of a *gfp* transgene by exposing adult animals to 15 μg/ml 1,1′-dioctadecyl-3,3,3′,3′-tetramethylindocarbocyanine perchlorate (DiI) in M9 buffer (Brenner, 1974) for 1.5 h to label ASJ along with the ADL, ASH, ASI, ASK, and AWB amphid chemosensory neuron pairs. The ASJ defects scored by the *tax-2*Δ*::gfp* transgene or DiI filling differed in penetrance by up to 20%, but in all cases qualitatively similar results were obtained with

the use of both *tax-2Δ::gfp* and DiI filling of strains lacking a *gfp* transgene.

Animals were scored as having ectopic neurite defects if at least one neuron had an ectopic thin or thick process that was longer than the diameter of the cell body. Lateral ectopic neurites emerged directly from the cell body in *sax-1* and *sax-2* mutants and grew posteriorly along the lateral body wall. *tax-4* mutants exhibit both lateral and ventral neurite defects in ASJ (Peckol *et al.*, 1999), whereas *sax-1* and *sax-2* mutants exhibit only lateral neurites. Only lateral neurites were included in this analysis. In Table 1, Figure 2, and Figure 5, ASE and AWC neurons were scored as defective in cell shape if the mutant cell body appeared at least twice the size of a wild-type cell body. Because *rhoA*-expressing cells had milder defects than *sax-1* mutants, in Figure 6 ASE neurons were scored as defective in cell shape if the cell body was expanded 1.5-fold compared with wild-type neurons.

Statistical analysis was conducted with the use of Primer of Biostatistics software (Stanton A. Glantz, McGraw-Hill, New York) and Kaleidagraph (Synergy Software, Reading, PA). Confocal images were acquired with the use of LaserSharp Acquisition version 2.1A software (Bio-Rad, Richmond, CA), an Optiphot-2 microscope (Nikon, Garden City, NY), and the MRC-1024 Laser Scanning Confocal Imaging System (Bio-Rad). Epifluorescence images were acquired with the use of an Axioplan 2 microscope (Zeiss, Thornwood, NY) and assembled with the use of Adobe Photoshop (Adobe, Mountain View, CA). The image in Figure 5D was acquired with a scientific-grade cooled charge-coupled device camera on a multiwavelength wide-field three-dimensional microscopy system (Hiraoka *et al.*, 1990).

sax-1 Expression Analysis

A full-length translational SAX-1::GFP fusion was constructed by cloning Green Fluorescent Protein (GFP) flanked by splice acceptor and donor sites (pPD103.75) into the blunted *Afl*II site in the last intron of the *Sac*II–*Xba*I *sax-1* genomic fragment in a pBSKII+ backbone. This SAX-1::GFP transgene (pJAZ31) was injected at 50 ng/μl into a *lin-15(n765ts)* strain with the use of 30 ng/μl pJM23 *lin-15* plasmid as a coinjection marker (Huang *et al.*, 1994). To assess whether the SAX-1::GFP tag was functional, SAX-1::GFP was injected at 100 ng/μl into *sax-1(ky211)* X and *sax-1(ky491)* X mutant animals with pRF4, and rescue of the ectopic neurite phenotype was scored by DiI filling. The *sax-1* expression pattern was characterized in animals that contained the SAX-1::GFP plasmid as an unstable extrachromosomal array. Chemosensory neurons were scored for rescue of ectopic neurite defects by DiI filling of transgenic animals.

The *srh-1::gfp* construct contained a 3-kb fragment of the *srh-1* promoter (cosmid R09F10 nucleotides 24,398–27,397) engineered by PCR to contain a 5′ *Sph*I site and a 3′ *Bam*HI site and cloned into the corresponding sites of the pPD95.77 GFP vector by Yongmei Zhang (Howard Hughes Medical Institute, University of California, San Francisco, CA). The *gcy-5* constructs contained a 2.7-kb fragment upstream of the *gcy-5* start codon engineered by PCR to contain a 5′ *Sph*I site and a 3′ *Bam*HI site and cloned into the corresponding sites of the pPD95.75 GFP vector. GFP vectors were kindly provided by A. Fire, S. Xu, J. Ahnn, and G. Seydoux (Carnegie Institution of Washington, Baltimore, MD).

A *Kpn*I site was engineered immediately upstream of the *sax-1* cDNA start codon by PCR. The complete *sax-1* cDNA was cut at the 5′ *Kpn*I site and the 3′ *Nae*I site in the *sax-1* 3′ UTR. The *sax-1* cDNA was joined to the downstream *unc-54* 3′ UTR (cut with *Eco*RI and blunted) and the upstream *srh-1* or *gcy-5* promoters (cut with *Kpn*I). *gcy-5::sax-1* was injected at 50 ng/μl with pRF4 into the *kyIs164 II; sax-1(ky491)* X strain. *srh-1::sax-1* was injected at 50 ng/μl with pRF4 into the *sax-1(ky491)* X strain and the *kyIs164 II; sax-1(ky491)* X strain.

To express the SAX-1::GFP tag in a single cell type, the full-length SAX-1::GFP clone with GFP in the final intron was cloned into the *srh-1::sax-1* fusion gene (pJAZ22) in two steps. The *srh-1::sax-1::gfp* fusion gene (pJAZ35) was injected at 100 ng/μl into wild-type N2 animals with pRF4, and ASJ morphology was scored by DiI filling.

Isolation of a sax-1 Deletion Mutant

A *sax-1* deletion mutation was isolated by PCR as described (Dernburg *et al.*, 1998). A deletion library of 10^6 genomes was constructed with the use of the ethyl methanesulfate (EMS) mutagen for half and UV/trimethylpsoralen for half of the library. Nested PCR primers were used to amplify a 3-kb fragment containing the *sax-1* kinase domain. A 1.7-kb deletion band was identified in a pool from the EMS part of the library and sequenced. A single animal homozygous for the deletion was isolated after three rounds of sib selection. The *sax-1(ky491)* X deletion mutant was outcrossed once by N2 and once by *lon-2(e678)* X.

Isolation and Mutagenesis of rhoA cDNA

A full-length cDNA of the *rhoA* gene (Chen and Lim, 1994) was amplified by PCR from hexamer-primed *C. elegans* cDNA (a gift of Mario de Bono, Howard Hughes Medical Institute, University of California, San Francisco, CA) with the use of the primers 5′GAAGTCGACACGAGTACGGGTGTTC and 3′CCATGGAATTAGAGAGAAGAAGAGCAGAC, which contained artificial *Sal*I and *Nco*I sites, respectively. The cDNA was subcloned into *Sal*I–*Nco*I sites of the vector pPD49.26, sequenced, and determined not to contain any PCR-induced mutations. The *gcy-5* promoter (Yu *et al.*, 1997) was subcloned into the *Sph*I–*Bam*HI sites of the same vector with the use of artificial primers to create the restriction sites. Point mutations Q63L, T19N, and D13T in the *rhoA* gene were generated with the use of the Quikchange kit (Stratagene, La Jolla, CA). After mutagenesis, the complete *rhoA* coding region was sequenced to confirm the presence of the desired mutation and the absence of other mutations. *rhoA* plasmids were injected at 50 ng/μl with *rol-6* as a cotransformation marker. *gcy-5::sax-1* was injected at 50 ng/μl with the D13T mutant, and the *gcy-5* promoter plasmid was injected at 50 ng/μl with the D13T mutant as a control.

ASER cell shape was scored in adult animals raised at 25°C with the use of the *kyIs164* transgene.

RESULTS

Mutations in sax-1 and sax-2 Disrupt Neuronal Cell Shape and Neurite Initiation

sax-1 and *sax-2* mutations cause ectopic neurite initiation from the ASI sensory neurons, the CAN neuroendocrine neurons, and *glr-1*–expressing interneurons (Zallen *et al.*, 1999). Characterization of *sax-1* and *sax-2* mutants with cell-specific GFP markers for the AWC, ASE, and ASJ sensory neurons revealed similar defects in neurite initiation as well as defects in neuronal cell shape (Figure 1, Table 1). In *sax-1* and *sax-2* mutant animals, axon guidance of chemosensory neurons in the embryo was normal, producing a bipolar neuron with one dendrite that connects to the tip of the nose and one axon that grows circumferentially in the nerve ring neuropil. However, some sensory neurons had an ectopic neurite in addition to the normal dendrite and axon (Figure 1, H and I). These ectopic neurites extended posteriorly from the cell body for up to 25 μm and were up to ~1 μm in diameter; a normal axon is 75 μm long and 0.1 μm in diameter. In addition, the sensory neuron cell bodies appeared expanded and irregular in shape (Figure 1, B, C, E, and F). The expanded regions of the cell body are flattened and extended, like lamellipodia, but their structures have not been characterized in detail. The three sensory neuron types exhibited a range of phenotypes, with primarily cell shape defects in the AWC and ASE neurons and ectopic neurites in the ASJ neurons (Table 1).

Despite the aberrant AWC morphology, *sax-1* and *sax-2* mutant animals generated nearly wild-type chemotaxis responses to at-

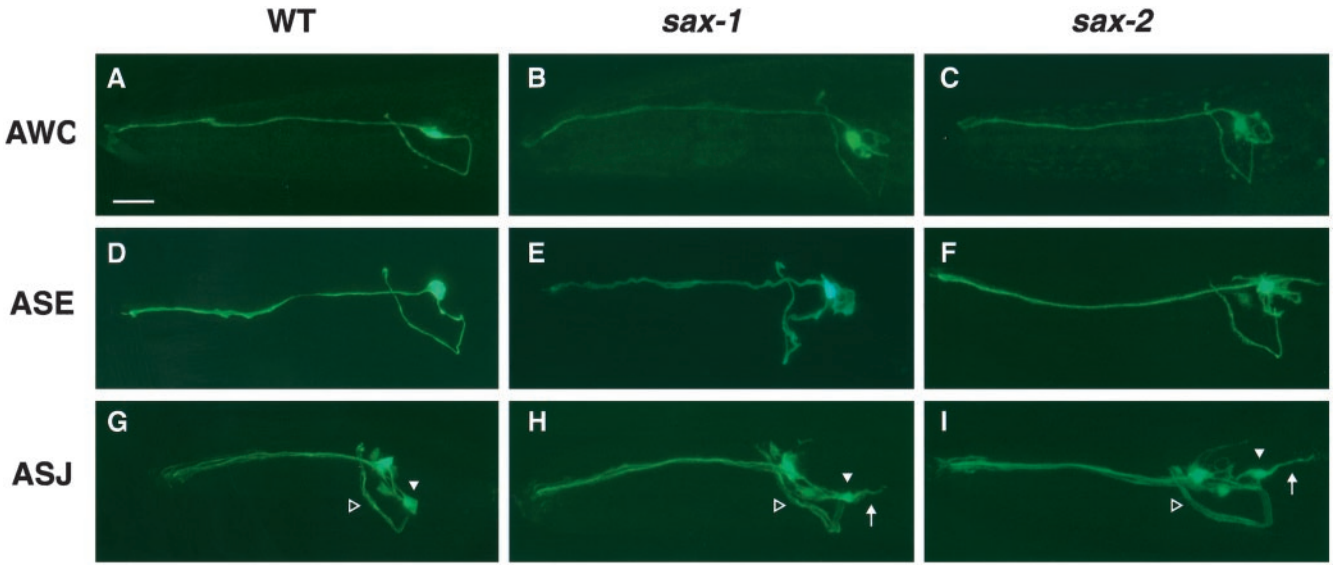

Figure 1. Morphological defects in amphid chemosensory neurons of *sax-1* and *sax-2* mutants. Each neuron extends one straight anterior dendrite and one U-shaped axon that enters the nerve ring. Neuronal morphology was characterized with integrated transgenes that express GFP in AWC (top row), ASER (middle row), and ASJ (bottom row, closed arrowheads). All panels show a lateral view of one side of the animal. Anterior is to the left, dorsal at top. Bar, 10 μm. Panels show wild-type (A, D, and G), *sax-1(ky211)* (B and H), s*ax-1(ky491)* (E), and *sax-2(ky216)* (C, F, and I) animals. The AWC and ASE neurons exhibited expanded and irregular cell shape defects in *sax-1* and *sax-2* mutants. The ASJ neurons produced ectopic, posteriorly misdirected neurites (H and I, arrows) in addition to the axon in the nerve ring (G, H, and I, open arrowheads). ASI neurons also have a normal axon in the nerve ring and a posterior ectopic neurite (Zallen *et al.*, 1999).

tractive odorants detected by AWC (Figure 2A), suggesting that these cell shape defects do not eliminate AWC function. *sax-1* and *sax-2* mutant animals appeared morphologically and behaviorally normal, with no obvious defects in locomotion or egg laying.

sax-1 and sax-2 Suppress Neurite Initiation in Larval and Adult Stages

The ectopic neurite phenotypes of *sax-1* and *sax-2* mutants are reminiscent of defects caused by mutations that disrupt the electrical activity of sensory neurons, which result in late-onset ectopic neurite initiation during larval and adult stages (Peckol *et al.*, 1999). To determine whether *sax-1* and *sax-2* also affect a late developmental process, we examined ectopic neurites in the ASJ sensory neurons at different larval stages. Although ASJ axon guidance is completed in the embryo, the ectopic neurites in *sax-1* and *sax-2* mutants increased in severity throughout the four larval stages and continued to appear in adults (Figure 2B). Activity mutants

Table 1. Some neuronal morphology defects in *sax-1* and *sax-2* mutants are temperature sensitive

	ASE[a]		ASJ[b]		AWC[c]	
	25°C	20°C	25°C	20°C	25°C	20°C
Wild type	2 (n = 110)	1 (n = 114)	4 (n = 154)	0 (n = 203)	0 (n = 136)	2 (n = 118)
sax-1(ky211)	84 (n = 102)[d]	43 (n = 106)	62 (n = 180)[d]	27 (n = 241)	92 (n = 129)[d]	68 (n = 287)
sax-1(ky491)	86 (n = 231)[d]	64 (n = 110)	59 (n = 286)[d]	13 (n = 214)	79 (n = 179)	86 (n = 332)
sax-2(ky216)	85 (n = 150)	89 (n = 131)	80 (n = 246)[d]	28 (n = 167)	97 (n = 150)	94 (n = 185)

Phenotypes were scored in adult animals raised at 25 or 20°C with the GFP fusion genes *gcy-5*::*gfp* (ASE), *tax-2*Δ::*gfp* (ASJ), and *str-2*::*gfp* (AWC). Animals with cell bodies greater than or equal to twice the normal size or with ectopic neurites longer than the diameter of the cell body were scored as defective. n, number of animals scored.

[a] *sax-1* and *sax-2* mutants exhibited predominantly cell shape defects in ASE and few ectopic neurites. For example, *sax-1(ky491)* at 25°C had 75% penetrant ASE cell shape defects and 11% penetrant ASE ectopic neurites (n = 231 animals).

[b] *sax-1* and *sax-2* mutants exhibited exclusively ectopic neurite defects in ASJ and no cell shape defects.

[c] *sax-1* and *sax-2* mutants exhibited predominantly cell shape defects in AWC and few ectopic neurites. For example, *sax-1(ky491)* at 25°C had 68% penetrant AWC cell shape defects and 12% penetrant AWC ectopic neurites (n = 179 animals).

[d] These values differ between 25 and 20°C at $p < 0.001$.

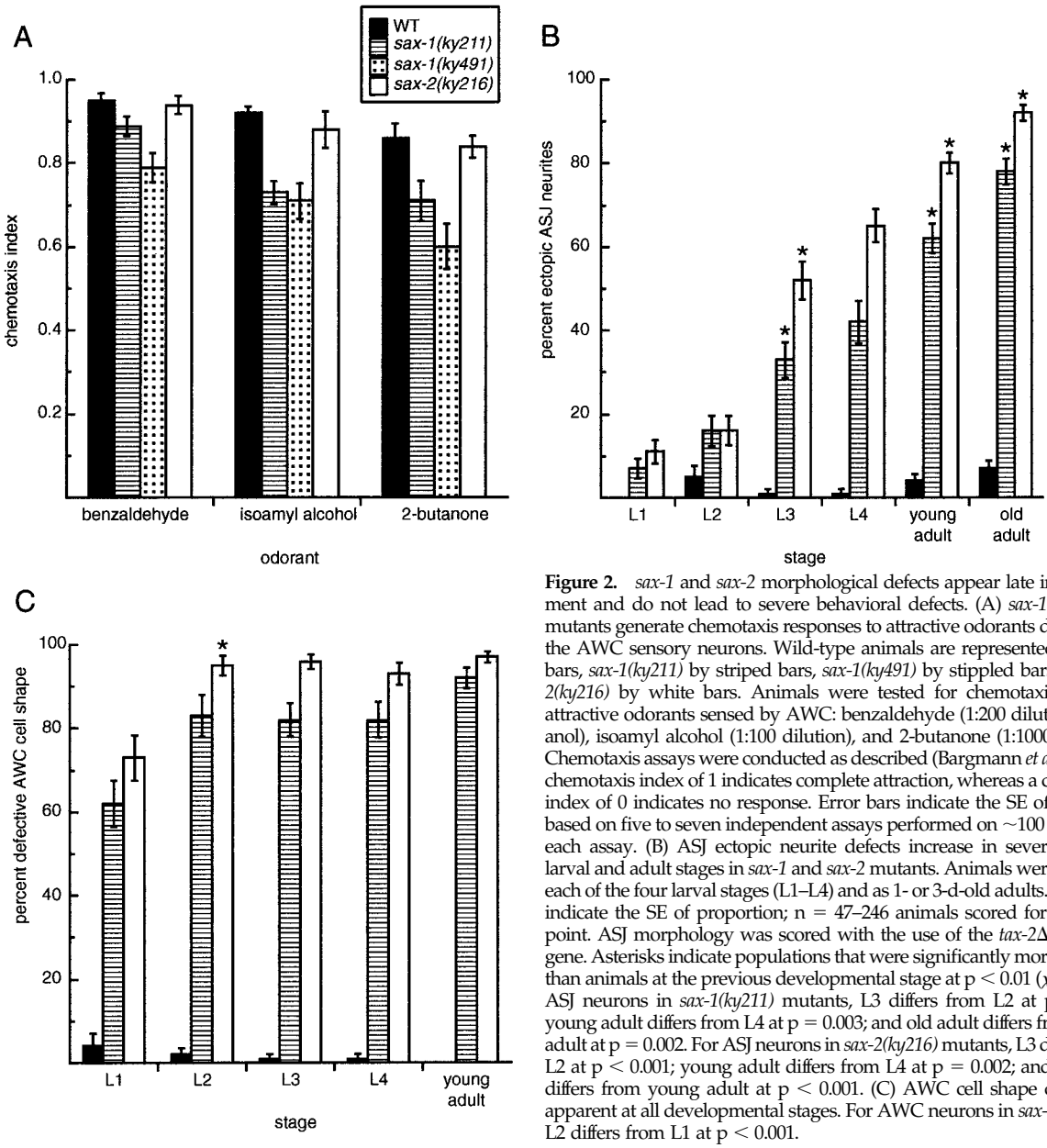

Figure 2. *sax-1* and *sax-2* morphological defects appear late in development and do not lead to severe behavioral defects. (A) *sax-1* and *sax-2* mutants generate chemotaxis responses to attractive odorants detected by the AWC sensory neurons. Wild-type animals are represented by black bars, *sax-1(ky211)* by striped bars, *sax-1(ky491)* by stippled bars, and *sax-2(ky216)* by white bars. Animals were tested for chemotaxis to three attractive odorants sensed by AWC: benzaldehyde (1:200 dilution in ethanol), isoamyl alcohol (1:100 dilution), and 2-butanone (1:1000 dilution). Chemotaxis assays were conducted as described (Bargmann *et al.*, 1993). A chemotaxis index of 1 indicates complete attraction, whereas a chemotaxis index of 0 indicates no response. Error bars indicate the SE of the mean based on five to seven independent assays performed on ~100 animals in each assay. (B) ASJ ectopic neurite defects increase in severity during larval and adult stages in *sax-1* and *sax-2* mutants. Animals were scored at each of the four larval stages (L1–L4) and as 1- or 3-d-old adults. Error bars indicate the SE of proportion; n = 47–246 animals scored for each data point. ASJ morphology was scored with the use of the *tax-2Δ::gfp* transgene. Asterisks indicate populations that were significantly more defective than animals at the previous developmental stage at $p < 0.01$ (χ^2 test). For ASJ neurons in *sax-1(ky211)* mutants, L3 differs from L2 at $p = 0.007$; young adult differs from L4 at $p = 0.003$; and old adult differs from young adult at $p = 0.002$. For ASJ neurons in *sax-2(ky216)* mutants, L3 differs from L2 at $p < 0.001$; young adult differs from L4 at $p = 0.002$; and old adult differs from young adult at $p < 0.001$. (C) AWC cell shape defects are apparent at all developmental stages. For AWC neurons in *sax-2* mutants, L2 differs from L1 at $p < 0.001$.

are also temperature-sensitive for ectopic neurite formation (Peckol *et al.*, 1999), and more ectopic neurites are observed in *sax-1* and *sax-2* mutants at higher temperatures (Table 1) (Zallen *et al.*, 1999).

Unlike ectopic neurites, the cell shape defects in *sax-1* and *sax-2* mutants are not observed in mutants with defects in sensory activity and have not been described previously in *C. elegans*. The AWC cell shape defects were apparent even at the L1 stage, although they increased slightly in severity between the first and second larval stages (Figure 2C). The ASE cell shape defects were temperature-sensitive in *sax-1* but not in *sax-2* mutants, whereas AWC cell shape defects were temperature-sensitive in only one *sax-1* allele (Table 1).

SAX-1 Acts in Parallel with the UNC-43 Calcium/Calmodulin-dependent Kinase and the TAX-4 Sensory Transduction Channel to Regulate Neurite Initiation

The ectopic neurite defects, late onset, and temperature-sensitivity of *sax-1* mutants were all similar to the defects in mutants with altered sensory transduction or electrical activity. To determine whether SAX-1 participates in an activity-dependent pathway, we generated double mutants defective in *sax-1* and the cGMP-gated sensory transduction channel *tax-4* (Komatsu *et al.*, 1996). ASJ neurons in the *sax-1; tax-4* double mutant displayed significantly more ectopic neurites than a null mutant in either gene (Figure 3A),

indicating that these genes function in two different pathways to suppress neurite initiation.

The SAX-1–related Ndr kinase can be regulated by calcium (Millward *et al.*, 1998; see below), and calcium-dependent kinases such as CaMKII have been implicated in the regulation of neuronal morphology in response to neural activity (Wang *et al.*, 1994; Wu and Cline, 1998). *C. elegans* has a single predicted CaMKII homologue encoded by the *unc-43* gene (Reiner *et al.*, 1999). To determine whether CaMKII is involved in the regulation of cell morphology in *C. elegans*, we examined chemosensory neurons in *unc-43* mutants. Both the null *unc-43(n1186lf)* mutation and the gain-of-function *unc-43(n498gf)* mutation caused occasional ectopic neurites in the ASJ (Figure 3B) and ASE neurons [13% defective in *unc-43(lf)*, n = 194; 3% defective in *unc-43(gf)*, n = 159], but no cell shape defects.

Genetic evidence indicates that the UNC-43 CaMKII functions in the activity-dependent pathway to regulate neurite initiation. The ASJ defects in the *tax-4; unc-43(lf)* double mutant were not enhanced compared with the *tax-4* single mutant (Figure 3B), suggesting that UNC-43 functions in the same pathway as the TAX-4 sensory transduction channel. The *tax-4; unc-43(gf)* double mutant was significantly suppressed for the *tax-4* ASJ defects, suggesting that UNC-43 acts downstream of TAX-4. However, *tax-4* null mutants were significantly more defective than *unc-43* null mutants at 25°C (Figure 3B), indicating that TAX-4 carries out additional UNC-43–independent functions.

UNC-43, like TAX-4, functions in parallel with the SAX-1 kinase. The ASJ neurons in the *sax-1; unc-43(lf)* double mutant were significantly more defective than in a null mutant in either gene, indicating that SAX-1 and UNC-43 operate in parallel pathways (Figure 3C). Interestingly, the *sax-1; unc-43(gf)* double mutant was partially suppressed compared with the *sax-1* single mutant at 25°C, suggesting that increased activity of the UNC-43 kinase can partially compensate for decreased SAX-1 kinase activity.

sax-1 and *sax-2* mutants have similar defects in neurite initiation and cell shape. The ASJ defects in *sax-1; sax-2* double mutants were no more severe than those in either single mutant (Figure 3D), suggesting that these genes act in the same genetic pathway. We conclude that SAX-1 and SAX-2 function together, at least partly in parallel with an activity-dependent pathway that regulates neurite initiation through the action of the TAX-4 sensory transduction channel and the UNC-43 CaMKII.

sax-1 Encodes an Ndr Serine/Threonine Protein Kinase

sax-1 was mapped to the X chromosome between the *stP40* polymorphism and the *lin-18* gene, and cosmid pools covering this region were injected into the *sax-1(ky211)* strain. The R11G1 cosmid and its subclones rescued *sax-1* mutant defects (Figure 4A). Sequence information from the *C. elegans* Sequencing Consortium predicted that the smallest rescuing subclone contained a serine/threonine kinase. A 1-kb deletion within the predicted kinase domain completely abolished rescuing activity (Figure 4A). To confirm that this gene was disrupted in *sax-1* mutant animals, we sequenced *sax-1(ky211)* and identified a G-to-A transition mutation in a predicted splice acceptor site. Fifteen full-length *sax-1* cDNAs from a mixed-stage *C. elegans* cDNA library (Barstead and Waterston, 1989) define a 1.8-kb primary transcript that encodes a predicted protein of 467 amino acids. An additional 2 amino acids were present at the 11th splice acceptor site in 1 of 15 clones. The 467-amino acid protein overlaps with the first third of the putative protein R11G1.4, which was predicted to encode a 1356-amino acid protein based on genomic sequence. The *sax-1* transcript was contained within the 7.7-kb rescuing subclone, which included 1.9 kb of upstream sequence and 2.4 kb of downstream sequence (Figure 4A).

sax-1 encodes a protein with homology to serine/threonine protein kinases, including the 11 highly conserved motifs that constitute the catalytic domain (Hanks *et al.*, 1988). The SAX-1 kinase belongs to a family of serine/threonine kinases that is conserved from yeast to humans (Figure 4, B and C). SAX-1 is most closely related to the Ndr kinases (Millward *et al.*, 1995), with 62% amino acid identity to human Ndr and 60% identity to *Drosophila* Ndr. Certain features distinguish Ndr kinases from other serine/threonine kinases, including a conserved N-terminal region and a 34- to 45-amino acid spacer between kinase motifs VII and VIII. Several close relatives of Ndr possess these features, including *Schizosaccharomyces pombe* Orb6, *Neurospora* COT-1, and *Drosophila* Warts/Lats (Yarden *et al.*, 1992; Justice *et al.*, 1995; Xu *et al.*, 1995; Verde *et al.*, 1998). However, the Ndr kinases form a distinct class: *C. elegans* has both SAX-1/Ndr and a Warts/Lats homologue (T20F10.1), and *Drosophila* has an Ndr kinase as well as Warts/Lats.

SAX-1 is related to Rho kinases (Figure 4C), with 35% amino acid identity and 52% amino acid similarity to human $p160^{ROCK}$/ROKβ. However, Rho kinases lack the SAX-1 spacer region between kinase subdomains VII and VIII, possess divergent N termini, and contain an additional C-terminal region that mediates Rho association (Leung *et al.*, 1995; Fujisawa *et al.*, 1996).

Immediately 3′ of the predicted *sax-1* gene lies a second predicted ORF with a C1 motif (phorbol ester/diacylglycerol binding) and a C2 motif (calcium binding) that was predicted to be part of the same R11G1.4 protein as SAX-1 by the *C. elegans* Sequencing Consortium. We found that this gene encodes a separate 811-amino acid protein that does not overlap with SAX-1 (see MATERIALS AND METHODS) and is not required for *sax-1* rescue. Its mRNA begins with an SL2 splice leader, suggesting that it may be in a common operon with *sax-1*.

Isolation of a Candidate sax-1 Null Mutation

The *sax-1(ky211)* mutation is predicted to disrupt *sax-1* splicing and may cause a partial or complete loss of gene function. To obtain a null allele of *sax-1*, we used a PCR-based strategy to isolate a deletion mutant from a library of 10^6 EMS- or UV-trimethylpsoralen–mutagenized animals (see MATERIALS AND METHODS). The *sax-1(ky491)* mutation represents a 1.3-kb deletion of genomic sequence that leads to a frame shift in the *sax-1* ORF early in the kinase domain. *sax-1(ky491)* is predicted to encode a truncated gene product containing only 3 of the 11 conserved kinase domains. Both break points of the deletion occur in exons, and the deleted sequences encompass conserved domains IV, V, and VIA of the *sax-1* kinase region. Based on the early frame shift and the complete elimination of conserved kinase sequences, *sax-1(ky491)* is a candidate null allele. The *sax-1(ky491)* dele-

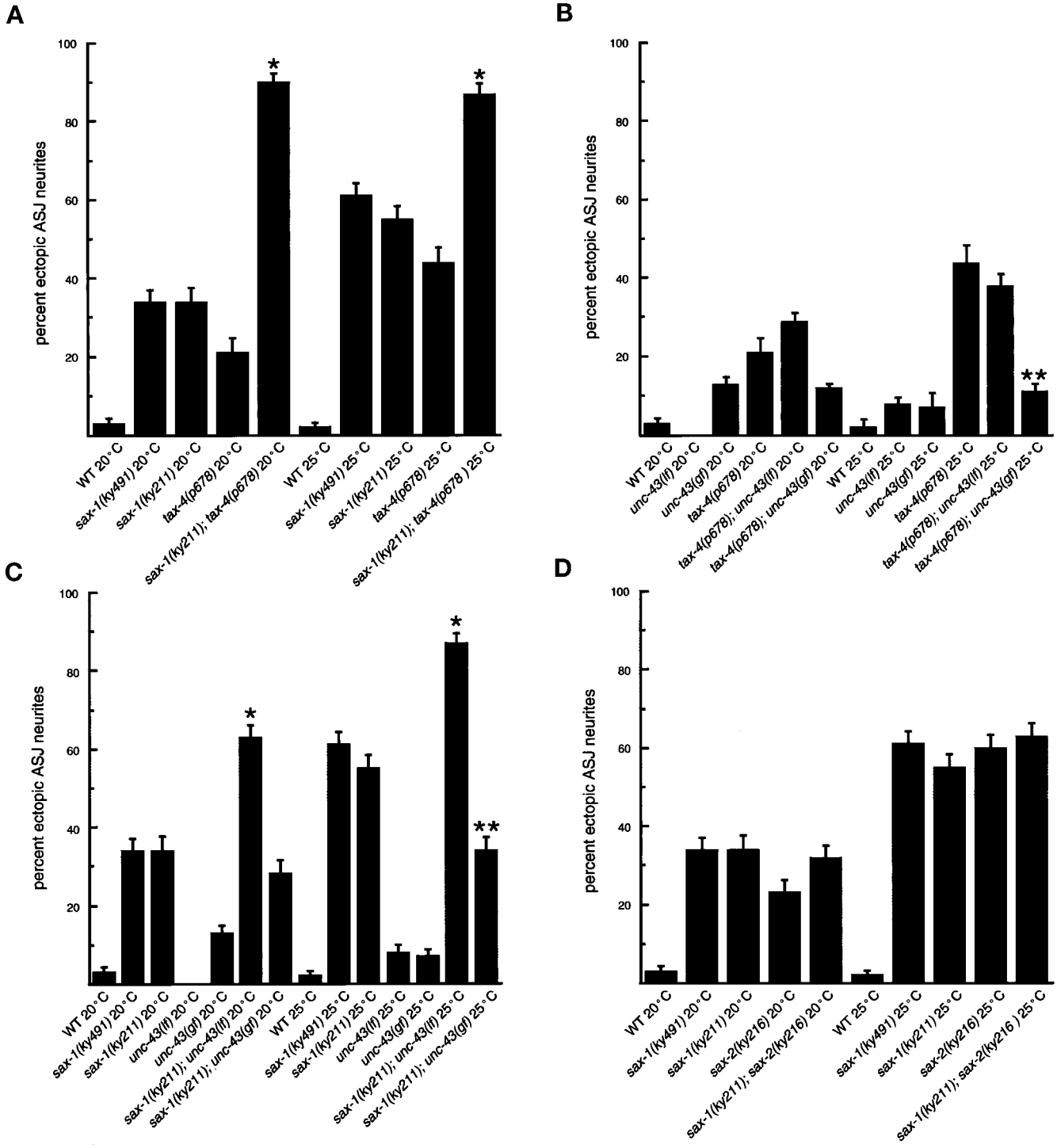

Figure 3. ASJ ectopic neurite defects in *sax-1*, *tax-4*, *unc-43*, and *sax-2* single and double mutants. (A) *sax-1* and *tax-4*. (B) *unc-43* and *tax-4*. (C) *sax-1* and *unc-43*. (D) *sax-1* and *sax-2*. Strains grown at 20°C are shown on the left of each panel, strains grown at 25°C are shown on the right. Error bars indicate the SE of proportion; n = 110–362 animals scored for each data point. ASJ morphology was scored with the use of DiI filling of animals lacking a *gfp* transgene; qualitatively similar results were obtained with *tax-2*Δ*::gfp*. Single asterisks indicate double mutants that were significantly more defective than either single mutant at that temperature ($p < 0.001$, χ^2 test). Double asterisks indicate double mutants that were significantly suppressed compared with the more severe single mutant at that temperature ($p < 0.001$, χ^2 test). *tax-4* mutant defects were less severe than those reported previously (Peckol *et al.*, 1999) because only lateral axon defects were included in this analysis (see MATERIALS AND METHODS).

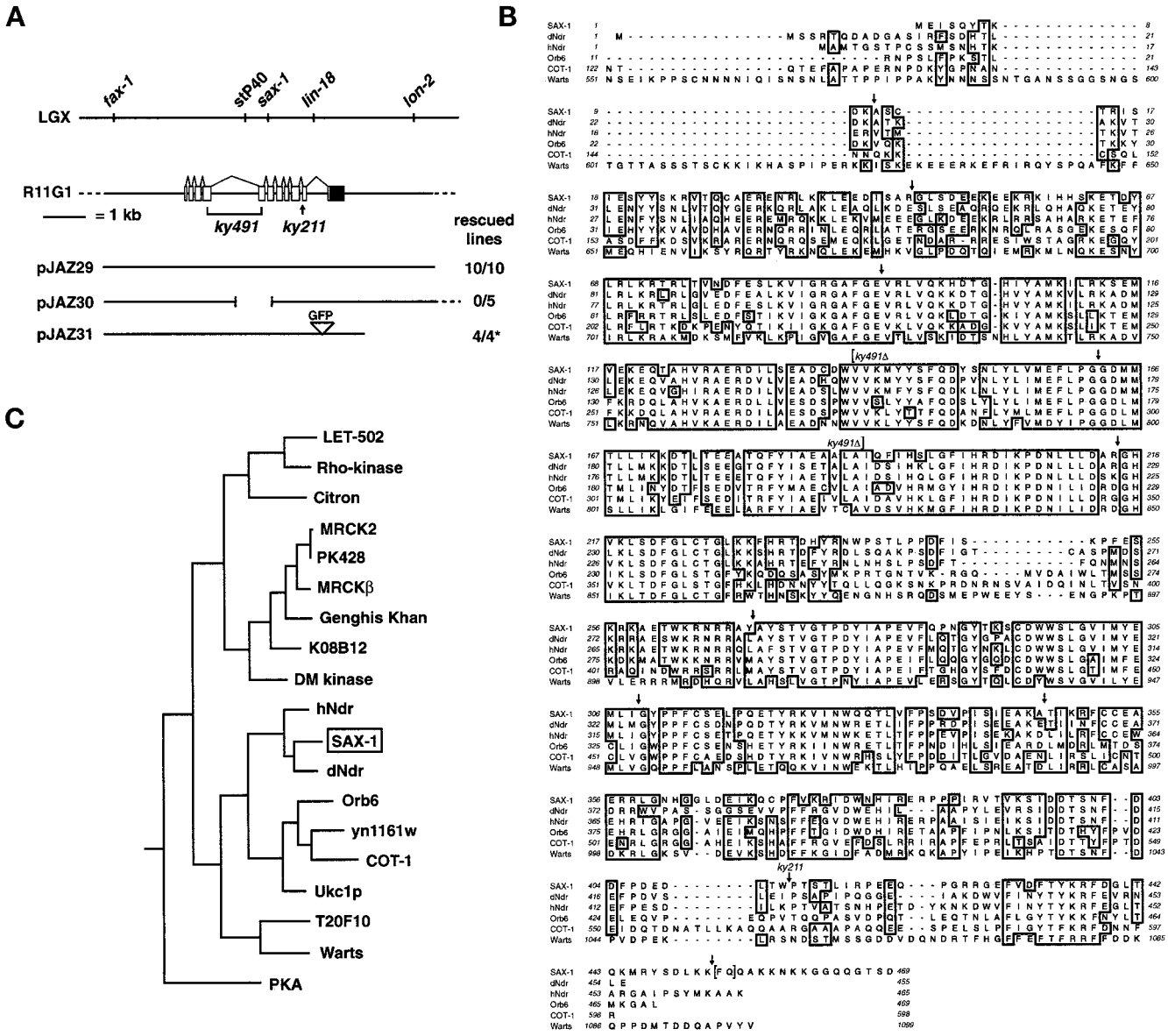

Figure 4. *sax-1* encodes a serine/threonine kinase. (A) The *sax-1* mutation mapped to LGX between the *stP40* and *lin-18* markers. *sax-1* mutant defects were rescued by the R11G1 cosmid and specific cosmid subclones. The exon/intron structure of the *sax-1* genomic region is shown; exons are open boxes, introns are lines, and the 3′ UTR is a closed box. Rescued lines indicate the number of independent transgenic *sax-1(ky211)* lines whose defects scored with the *ceh-23::gfp* transgene (pJAZ29 and pJAZ30) or by DiI filling (pJAZ31) were rescued by the specified plasmid (see MATERIALS AND METHODS). The asterisk indicates that two of two *sax-1(ky211)* transgenic lines and two of two *sax-1(ky491)* transgenic lines were rescued. (B) Alignment of the SAX-1 protein sequence with sequences of the *Drosophila* and human Ndr kinases (dNdr and hNdr), *S. pombe* Orb6, *Neurospora* COT-1, and *Drosophila* Warts/Lats. Conserved residues that are shared by four or more proteins are boxed. Arrows indicate splice junctions in *sax-1*. Brackets denote the beginning and end of the *ky491* deletion, which also causes a frame shift that results in *sax-1* termination early in the kinase domain. Sequences were aligned with the use of Clustal W. (C) Phylogenetic tree indicating the relationship between the kinase catalytic domains of SAX-1 and other serine/threonine kinases. Rho-kinase is p160ROCK/rokβ. Sequences were analyzed with the use of the Phylip/PAUP Genetics Computer Group (Madison, WI) sequence analysis programs.

tion mutation was fully recessive and caused defects similar to those caused by the *sax-1(ky211)* allele (Table 1, Figures 1E and 2A), indicating that the partially penetrant, temperature-sensitive defects in the ASJ and ASE neurons represent the *sax-1* null phenotype.

A SAX-1::GFP Translational Fusion Is Broadly Expressed in Neurons, Hypodermis, and Muscle

To determine the pattern of *sax-1* expression, we inserted a *gfp* reporter flanked by splice sites into the final *sax-1* intron, 15

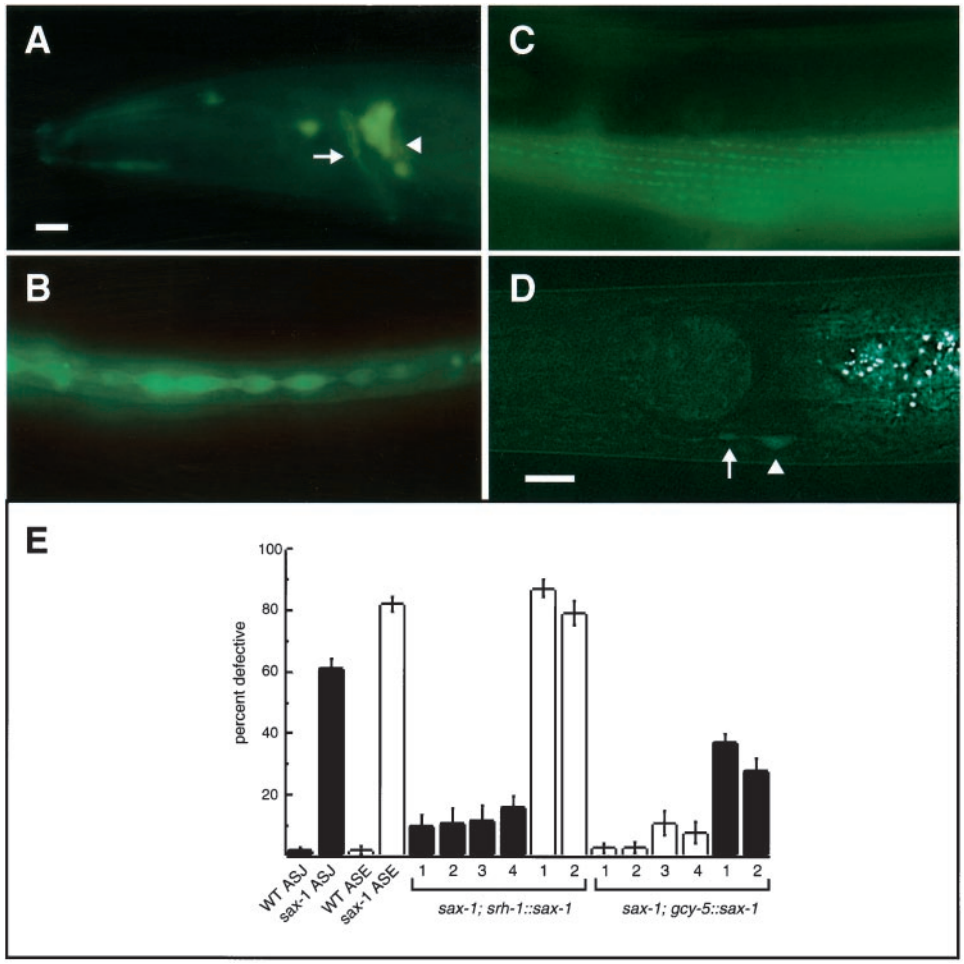

Figure 5. SAX-1::GFP expression and site of action. SAX-1::GFP expression is shown in larval (B) and adult (A, C, and D) animals. All panels show a lateral view of one side of the animal. Anterior is to the left, dorsal at top. Bars, 10 μm. (A) SAX-1::GFP is expressed in lateral ganglion neurons in the head of the animal (arrowhead) that contribute axons to the nerve ring (arrow). (B) SAX-1::GFP labels lateral seam cells in the epidermis. (C) The SAX-1::GFP tag displays a punctate localization in muscle, shown here in body wall muscle in the midbody of the animal. This pattern is relatively common for GFP fusion genes, and its significance is unknown. (D) The *srh-1::sax-1::gfp* tagged fusion was detected throughout the cell body of the ASJ neuron type (arrowhead) and occasionally in the proximal axon and dendrite (arrow). (E) SAX-1 is likely to function cell autonomously in the ASJ and ASE chemosensory neurons. ASJ ectopic neurite defects are represented by black bars and ASE cell shape defects are represented by white bars. ASJ was scored with the use of DiI filling. Error bars indicate the SE of proportion; n = 46–307 animals scored for each data point. Expression of the *srh-1::sax-1::gfp* transgene in ASJ rescued the ASJ defects of *sax-1(ky491)* mutants (four independent transgenic lines) but not the ASE defects (two independent transgenic lines). Expression of the *gcy-5::sax-1* transgene in ASE rescued the ASE defects of *sax-1(ky491)* mutants (four independent transgenic lines) and partially rescued the ASJ defects (two independent transgenic lines). All rescued lines were significantly different from *sax-1(ky491)* animals ($p < 0.001$, χ^2 test).

amino acids before the stop codon. The SAX-1::GFP fusion contained all exons, introns, and 5′ regulatory regions present in the rescuing *sax-1* subclone. The SAX-1::GFP tag rescued the ASJ defects of *sax-1(ky211)* and *sax-1(ky491)* mutant animals (Figure 4A). SAX-1::GFP was widely expressed in embryos and continued to be expressed in larvae in neurons that contribute axons to the nerve ring (Figure 5A), hypodermal cells, including lateral seam cells (Figure 5B), and muscle, where the SAX-1::GFP tag displayed a punctate localization (Figure 5C). The rescuing SAX-1::GFP fusion was present in the nucleus and cytoplasm of cells (Figure 5, A–D).

Although they express SAX-1::GFP, hypodermal seam cells do not have obvious defects in *sax-1* mutants. They secrete normal alae, indicating a correct apical/basal polarity, and have an apparently normal cell shape as assessed by expression of the cell junction marker JAM-1::GFP (Mohler *et al.*, 1998).

sax-1 Can Function Cell Autonomously to Regulate Cell Shape

Because SAX-1::GFP is broadly expressed, we wanted to determine whether SAX-1 functions cell autonomously in chemosensory neurons to regulate cell shape and neurite initiation. We used the *gcy-5* promoter (Yu *et al.*, 1997) to drive *sax-1* expression in the right ASE neuron. *gcy-5::sax-1* expressed in ASER was able to fully rescue the ASER defects of *sax-1* null mutant animals (Figure 5E), suggesting that SAX-1 can function cell autonomously to regulate ASER cell shape. However, the ASJ ectopic neurite defects were also partially rescued in these animals (Figure 5E). These results are consistent with two possibilities: SAX-1 could function cell autonomously in ASER and nonautonomously in ASJ, or the *gcy-5* promoter may be expressed at a low level in ASJ, allowing partial ASJ rescue.

To determine whether SAX-1 can function cell autonomously in ASJ to repress neurite initiation, we used an independent promoter to express SAX-1 in ASJ but not in ASE. The promoter for the predicted seven-transmembrane-domain receptor *srh-1* drives expression in the two ASJ sensory neurons and pharyngeal muscle (Y. Zhang and C.I.B., unpublished results). Expression of the *sax-1* cDNA from the *srh-1* promoter fully rescued the ectopic neurite defects in the ASJ neurons of *sax-1(ky491)* null mutant ani-

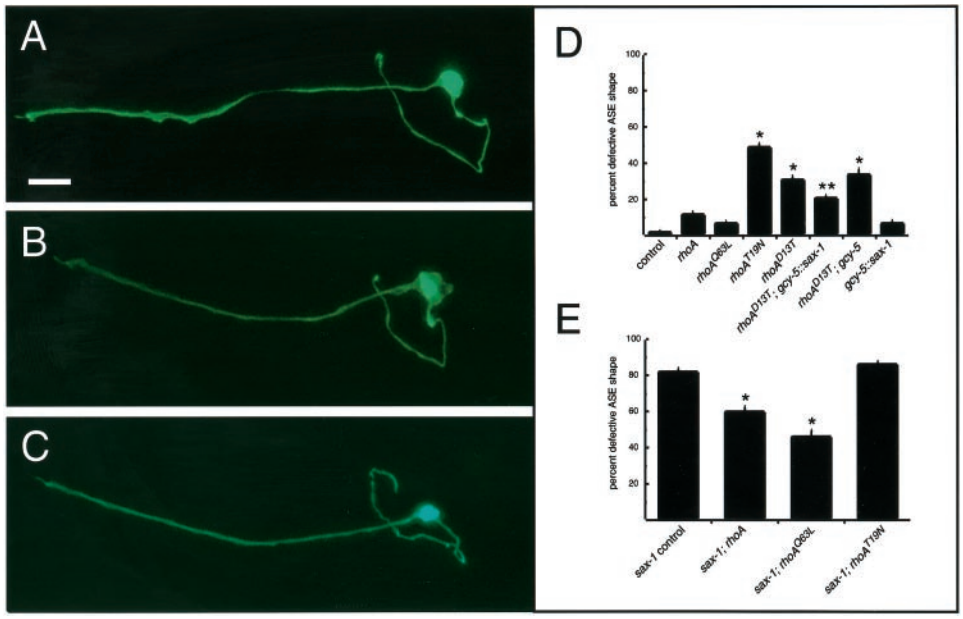

Figure 6. ASER cell shape is altered by expression of *rhoA* mutant alleles. Neuronal morphology was characterized with the *gcy-5::gfp* transgene. All panels show a lateral view of one side of the animal. Anterior is to the left, dorsal at top. Bar, 10 μm. (A) ASER morphology in a wild-type animal. (B) Expanded cell shape defect in an animal expressing $rhoA^{D13T}$ in ASER. Note that this defect is milder than typical *sax-1* defects (Figure 1). (C) Wild-type morphology in an animal overexpressing both $rhoA^{D13T}$ and *sax-1* in ASER. (D and E) Effects of *rhoA* (wild type), $rhoA^{Q63L}$ (predicted gain of function), $rhoA^{T19N}$ (predicted dominant negative), or $rhoA^{D13T}$ (predicted dominant negative) expression on ASER cell shape in wild-type and mutant backgrounds. *rhoA* defects were weaker than those of *sax-1* mutants. When scored by the criteria used for *sax-1* in Figures 2, 3, and 5 (a twofold increase in cell size), the *rhoA* mutants did not cause significant defects (cells expressing GFP alone were 2% defective, cells expressing *rhoA* cDNAs were 4–8% defective). Therefore, a less stringent criterion of a 1.5-fold increase was used to score *rhoA* defects. By this criterion, *sax-1* mutant severity did not change (compare Figure 6E to Figures 2, 3, and 5), but significant *rhoA* phenotypes could be detected. (D) Expression of *rhoA* alleles in wild-type animals. Significant cell shape defects (asterisks) were observed in ASER after expression of the predicted dominant negative $rhoA^{T19N}$ and $rhoA^{D13T}$ transgenes (single asterisks, $p < 0.001$, χ^2 test). Overexpression of *sax-1* in ASER with the use of the *gcy-5* promoter partly suppressed the dominant negative effect of $rhoA^{D13T}$ (double asterisk, different from both control and $rhoA^{D13T}$ lines at $p < 0.001$, χ^2 test). The *gcy-5* promoter alone did not suppress the $rhoA^{D13T}$ defects. (E) Expression of *rhoA* alleles in *sax-1(ky491)* animals. The *rhoA* (wild type) and $rhoA^{Q63L}$ (predicted gain of function) alleles partly suppressed the *sax-1* defect ($p < 0.001$, χ^2 test). The predicted dominant negative $rhoA^{T19N}$ allele did not enhance the *sax-1* defect. Control animals were injected with the coinjection marker alone. All phenotypes were scored at 25°C. Error bars indicate the SE of proportion, combining animals from four independent transgenic lines; $n > 50$ animals scored for each line.

mals but did not rescue the ASER defects (Figure 5E). To determine whether rescuing activity was due to *sax-1* expression in ASJ or in pharyngeal muscle, we coinjected the *srh-1::sax-1* transgene and an *srh-1::gfp* fusion to form an unstable extrachromosomal array whose site of expression can be monitored by *gfp* fluorescence. Mosaic animals with *gfp* expression in ASJ but not in the pharyngeal muscle were rescued for the ASJ defects (14 of 15 mosaic animals rescued). This result suggests that *sax-1* expression in ASJ is sufficient for ASJ rescue, indicating that SAX-1 is likely to function cell autonomously in ASJ to regulate neurite initiation.

An *srh-1::sax-1::gfp* tag also rescued the ASJ ectopic neurite defects of *sax-1* mutants [three independent transgenic lines: 10–12% defective, n = 46–80, each line significantly rescued at $p < 0.001$; control *sax-1(ky491)* animals: 61% defective, n = 218]. In larval and adult animals, SAX-1::GFP fluorescence was detected throughout the ASJ cell body, including the nucleus and the cytoplasm, and occasionally in the proximal axon and dendrite (Figure 5D).

The C. elegans RhoA GTPase Can Influence Neuronal Cell Shape

SAX-1 belongs to a kinase family that includes the Rho kinases, but its targets are unknown. To determine whether SAX-1 might have functions similar to those of the Rho kinases, we explored the activity of the *C. elegans* RhoA GTPase in sensory neurons. *C. elegans* RhoA shares 87% identity with vertebrate RhoA GTPases and is expressed in nerve ring neurons during larval stages (Chen and Lim, 1994). Use of RNA interference to disrupt *rhoA* function caused embryonic lethality (E.A. Lundquist and C.I.B., unpublished observations), precluding a straightforward loss-of-function analysis. Therefore, we generated mutations in conserved residues in the *rhoA* ORF that are predicted to confer dominant negative ($rhoA^{T19N}$) or gain-of-function ($rhoA^{Q63L}$) properties (Feig and Cooper, 1988; Bourne *et al.*, 1991). Wild-type *rhoA*, $rhoA^{T19N}$, and $rhoA^{Q63L}$ were expressed from the *gcy-5* promoter (Yu *et al.*, 1997) to drive expression in the ASER chemosensory neuron in late embryonic-, larval-, and adult-stage animals. The $rhoA^{T19N}$ allele, which is predicted to reduce endogenous *rhoA* function, caused ASER cell shape defects that resembled those of *sax-1* mutant animals (Figure 6D). A second mutation in the GTP-binding domain, $rhoA^{D13T}$, also caused cell shape defects (Figure 6, B and D), suggesting that this allele also functions in a dominant negative manner. Minimal defects were caused by expression of *rhoA* or $rhoA^{Q63L}$ (Figure 6D). These results suggest that RhoA-dependent pathways can regulate cell shape in chemosensory neurons. However, the defects observed in *rhoA*-expressing animals were less marked than those in

sax-1 mutants. Whereas *sax-1* mutant cell bodies were usually more than twice as large as wild type, the *rhoA*^{T19N} or *rhoA*^{D13T} cell bodies were rarely more than 1.5-fold larger than wild type.

A *sax-1; rhoA*^{T19N} strain had defects that were no more severe than the *sax-1* single mutant, suggesting that *sax-1* and *rhoA* affect a similar process (Figure 6E). In agreement with this model, overexpression of *sax-1* partly suppressed *rhoA*^{D13T} defects (Figure 6, C and D), and overexpression of *rhoA* or *rhoA*^{Q63L} partly suppressed *sax-1* defects (Figure 6E).

DISCUSSION

The SAX-1 Ndr Kinase Regulates Neuronal Cell Shape

During normal development, neurite outgrowth is limited to discrete axons and dendrites, and the compact neuronal cell body is refractory to neurite initiation. In *sax-1* mutants, chemosensory neurons and other neuron types have an extended, irregularly shaped cell body and ectopic neurite-like processes. *sax-1* activity may stabilize neuronal morphology, maintain cell polarity, or localize factors that make the rigid cell body distinct from the exploratory axons. *sax-1* encodes a serine/threonine kinase related to the *Drosophila* and human Ndr kinases (Millward *et al.*, 1995) in a kinase family that includes *S. pombe* Orb6, *Neurospora* COT-1, and *Drosophila* Warts/Lats. The function of the Ndr kinase subfamily has not been analyzed previously, but Orb6, COT-1, and Warts/Lats all influence cell shape (Yarden *et al.*, 1992; Justice *et al.*, 1995; Xu *et al.*, 1995; Verde *et al.*, 1998), suggesting that these kinases participate in an evolutionarily conserved mechanism that regulates cell morphology. SAX-1 is the first member of this family found to affect neurons.

SAX-1 and related kinases may preferentially affect particular subcellular compartments or cell types. *sax-1* mutants have abnormal cell bodies, but axon and dendrite guidance in the same neurons appears to be normal. *Drosophila warts/lats* mutants exhibit localized epithelial cell shape defects, with abnormal apical surfaces but normal basolateral morphologies (Justice *et al.*, 1995). *C. elegans*, *Drosophila*, and humans all have both an *ndr/sax-1*–like gene and a *warts/lats*-like gene, suggesting that these two kinases have distinct functions. *sax-1* defects become more severe as animals mature, suggesting an ongoing requirement for SAX-1 kinase activity in the maintenance of cell morphology. The fission yeast Orb6 kinase is similarly required for cell shape maintenance; arrested elongate cells become spherical when *orb-6* function is disrupted (Verde *et al.*, 1995). Warts/Lats and Orb6 play an additional role in cell division (Justice *et al.*, 1995; Xu *et al.*, 1995; Verde *et al.*, 1998; St. John *et al.*, 1999), but we have not observed cell proliferation defects in *sax-1* mutants.

The functions of SAX-1 in *C. elegans* are reminiscent of the activities of RhoA GTPase in cultured mammalian neurons: inactivation of RhoA promotes cell flattening and neurite outgrowth, whereas activation of RhoA causes cell rounding and decreased neurite outgrowth (Jalink *et al.*, 1994; Gebbink *et al.*, 1997). The effect of RhoA on neurite outgrowth has been shown to be mediated by Rho kinase (Amano *et al.*, 1998; Hirose *et al.*, 1998; Katoh *et al.*, 1998). We found that dominant negative *rhoA* alleles or mutations in the SAX-1 kinase caused similar cell shape changes in *C. elegans* sensory neurons. Our genetic results are consistent with a model in which SAX-1 and RhoA act in a common process affecting cell shape. These experiments should be interpreted with caution, because they involve overexpression of wild-type and mutant proteins. However, standard genetic analysis of this pathway is likely to be difficult, because RNA interference of *rhoA* resulted in early embryonic lethality (E. Lundquist and C.I.B., unpublished data). Mutations in other GTPase pathways, including the *C. elegans* MIG-2 GTPase or the UNC-73 Dbl-homology exchange factor (Zipkin *et al.*, 1997; Steven *et al.*, 1998), do not cause cell shape defects in ASER, indicating that the effects of RhoA expression on cell shape are selective.

We propose that SAX-1, like Rho GTPase and Rho kinase, regulates the cytoskeleton in neuronal cells to inhibit cell spreading and neurite initiation. Human Ndr kinase localizes primarily to the nucleus in cultured cells, but a subpopulation of human Ndr protein is present at the cell periphery, where it could interact with the cytoskeleton (Millward *et al.*, 1995). Orb6/COT-1/Warts family kinases are related to Rho kinases but do not contain a Rho-binding domain and other regulatory domains. It is possible that SAX-1 and Rho kinases can phosphorylate similar targets but are regulated differently.

SAX-1 Functions in Parallel with an Activity-dependent Pathway Mediated by the UNC-43 Calcium/Calmodulin-regulated Kinase

The SAX-1 kinase functions in parallel with an activity-dependent pathway to inhibit neurite initiation in sensory neurons. Ectopic chemosensory neurites appear late in development in mutants with abnormal sensory transduction, ion channel function, or development of the dendritic sensory endings (Coburn and Bargmann, 1996; Coburn *et al.*, 1998; Peckol *et al.*, 1999). The *C. elegans unc-43* gene encodes CaMKII (Reiner *et al.*, 1999), and we observed mild neurite defects in *unc-43* mutants. Double-mutant analysis suggests that the calcium-permeable sensory channel TAX-4 functions upstream of the UNC-43 CaMKII in the activity-dependent pathway. CaMKII has also been implicated in the activity-dependent regulation of axonal and dendritic branching in flies and vertebrates (Budnik *et al.*, 1990; Wang *et al.*, 1994; Wu and Cline, 1998).

Although the ectopic neurite defects in *sax-1* and activity mutants are similar, double-mutant analysis argues that the SAX-1 kinase functions at least partly in parallel with TAX-4/UNC-43, not in an identical pathway. Moreover, the activity-dependent pathway affects only neurite initiation, whereas SAX-1 also regulates cell shape. The human Ndr kinase is regulated by calcium through a domain that is conserved in SAX-1 (Millward *et al.*, 1998), suggesting that SAX-1, like UNC-43, might respond to neuronal activity and calcium. Alternatively, these two pathways may represent activity-dependent (TAX-4 and UNC-43) and activity-independent (SAX-1) mechanisms that maintain sensory neuron morphology.

Interestingly, increased activity of the UNC-43 CaMKII can partially compensate for decreased activity of SAX-1,

perhaps by regulating a common downstream target. SAX-1/Ndr targets are unknown, but the related Rho kinase and CaMKII both phosphorylate the same residue on myosin light chain (Edelman *et al.*, 1990; Amano *et al.*, 1996). Phosphorylated myosin can regulate actin assembly and inhibit neurite extension (Tan *et al.*, 1992; Wang *et al.*, 1996), so this is one candidate among many that could be regulated by SAX-1 and UNC-43. The characterization of SAX-2 and other components of the SAX-1 pathway should provide further insight into the mechanisms that regulate neuronal morphology.

ACKNOWLEDGMENTS

We are grateful to Orion Weiner and John Sedat for deconvolution microscopy of the SAX-1::GFP fusion, Jeff Simske, Yongmei Zhang, Andy Fire, and Emily Troemel for GFP markers, and Rachel Kindt, Orion Weiner, and Maria Gallegos for comments on the manuscript and useful advice during the course of this work. Some of the strains used in this study were obtained from the *Caenorhabditis* Genetics Center. This work was supported by the Howard Hughes Medical Institute. J.A.Z. and D.M.T. were predoctoral fellows of the National Science Foundation. E.L.P. was supported by a research fellowship from the American Heart Association, California Affiliate. C.I.B. is an Investigator of the Howard Hughes Medical Institute.

REFERENCES

Amano, M., Chihara, K., Kimura, K., Fukata, Y., Nakamura, N., Matsuura, Y., and Kaibuchi, K. (1997). Formation of actin stress fibers and focal adhesions enhanced by Rho-kinase. Science *275*, 1308–1311.

Amano, M., Chihara, K., Nakamura, N., Fukata, Y., Yano, T., Shibata, M., Ikebe, M., and Kaibuchi, K. (1998). Myosin II activation promotes neurite retraction during the action of Rho and Rho-kinase. Genes Cells *3*, 177–188.

Amano, M., Ito, M., Kimura, K., Fukata, Y., Chihara, K., Nakano, T., Matsuura, Y., and Kaibuchi, K. (1996). Phosphorylation and activation of myosin by Rho-associated kinase (Rho-kinase). J. Biol. Chem. *271*, 20246–20249.

Bargmann, C.I., Hartwieg, E., and Horvitz, H.R. (1993). Odorant-selective genes and neurons mediate olfaction in *C. elegans*. Cell *74*, 515–527.

Barstead, R.J., and Waterston, R.H. (1989). The basal component of the nematode dense-body is vinculin. J. Biol. Chem. *264*, 10177–10185.

Bourne, H.R., Sanders, D.A., and McCormick, F. (1991). The GTPase superfamily: conserved structure and molecular mechanism. Nature *349*, 117–127.

Brenner, S. (1974). The genetics of *Caenorhabditis elegans*. Genetics *77*, 71–94.

Budnik, V., Zhong, Y., and Wu, C.F. (1990). Morphological plasticity of motor axons in *Drosophila* mutants with altered excitability. J. Neurosci. *10*, 3754–3768.

C. elegans Sequencing Consortium. (1998). Genome sequence of the nematode *C. elegans*: a platform for investigating biology. Science *282*, 2012–2018.

Chen, W., and Lim, L. (1994). The *Caenorhabditis elegans* small GTP-binding protein RhoA is enriched in the nerve ring and sensory neurons during larval development. J. Biol. Chem. *269*, 32394–32404.

Coburn, C.M., and Bargmann, C.I. (1996). A putative cyclic nucleotide-gated channel is required for sensory development and function in *C. elegans*. Neuron *17*, 695–706.

Coburn, C.M., Mori, I., Ohshima, Y., and Bargmann, C.I. (1998). A cyclic nucleotide-gated channel inhibits sensory axon outgrowth in larval and adult *C. elegans*: a distinct pathway for maintenance of sensory axon structure. Development *125*, 249–258.

Dernburg, A.F., McDonald, K., Molder, G., Barstead, R., Dresser, M., and Villeneuve, A.M. (1998). Meiotic recombination in *C. elegans* initiates by a conserved mechanism and is dispensable for homologous chromosome synapsis. Cell *94*, 387–398.

Di Cunto, F., Calautti, E., Hsiao, J., Ong, L., Topley, G., Turco, E., and Dotto, G.P. (1998). Citron rho-interacting kinase, a novel tissue-specific ser/thr kinase encompassing the Rho-Rac-binding protein Citron. J. Biol. Chem. *273*, 29706–29711.

Dwyer, N.D., Troemel, E.R., Sengupta, P., and Bargmann, C.I. (1998). Odorant receptor localization to olfactory cilia is mediated by ODR-4, a novel membrane-associated protein. Cell *93*, 455–466.

Edelman, A.M., Lin, W.H., Osterhout, D.J., Bennett, M.K., Kennedy, M.B., and Krebs, E.G. (1990). Phosphorylation of smooth muscle myosin by type II Ca^{2+}/calmodulin-dependent protein kinase. Mol. Cell. Biochem. *97*, 87–98.

Feig, L.A., and Cooper, G.M. (1988). Relationship among guanine nucleotide exchange, GTP hydrolysis, and transforming potential of mutated ras proteins. Mol. Cell. Biol. *8*, 2472–2478.

Fujisawa, K., Fujita, A., Ishizaki, T., Saito, Y., and Narumiya, S. (1996). Identification of the Rho-binding domain of p160ROCK, a Rho-associated coiled-coil containing protein kinase. J. Biol. Chem. *271*, 23022–23028.

Gebbink, M.F., Kranenburg, O., Poland, M., van Horck, F.P., Houssa, B., and Moolenaar, W.H. (1997). Identification of a novel, putative Rho-specific GDP/GTP exchange factor and a RhoA-binding protein: control of neuronal morphology. J. Cell Biol. *137*, 1603–1613.

Hall, A. (1994). Small GTP-binding proteins and the regulation of the actin cytoskeleton. Annu. Rev. Cell Biol. *10*, 31–54.

Hanks, S.K., Quinn, A.M., and Hunter, T. (1988). The protein kinase family: conserved features and deduced phylogeny of the catalytic domains. Science *241*, 42–52.

Hiraoka, Y., Sedat, J.W., and Agard, D.A. (1990). Determination of three-dimensional imaging properties of a light microscope system: partial confocal behavior in epifluorescence microscopy. Biophys. J. *57*, 325–333.

Hirose, M., Ishizaki, T., Watanabe, N., Uehata, M., Kranenburg, O., Moolenaar, W.H., Matsumura, F., Maekawa, M., Bito, H., and Narumiya, S. (1998). Molecular dissection of the Rho-associated protein kinase (p160ROCK)-regulated neurite remodeling in neuroblastoma N1E-115 cells. J. Cell Biol. *141*, 1625–1636.

Huang, L.S., Tzou, P., and Sternberg, P.W. (1994). The *lin-15* locus encodes two negative regulators of *Caenorhabditis elegans* vulval development. Mol. Biol. Cell *5*, 395–412.

Ishizaki, T., Maekawa, M., Fujisawa, K., Okawa, K., Iwamatsu, A., Fujita, A., Watanabe, N., Saito, Y., Kakizuka, A., Morii, N., and Narumiya, S. (1996). The small GTP-binding protein Rho binds to and activates a 160 kDa Ser/Thr protein kinase homologous to myotonic dystrophy kinase. EMBO J. *15*, 1885–1893.

Ishizaki, T., Naito, M., Fujisawa, K., Maekawa, M., Watanabe, N., Saito, Y., and Narumiya, S. (1997). p160ROCK, a Rho-associated. coiled-coil forming protein kinase, works downstream of Rho and induces focal adhesions. FEBS Lett. *404*, 118–124.

Jalink, K., van Corven, E.J., Hengeveld, T., Morii, N., Narumiya, S., and Moolenaar, W.H. (1994). Inhibition of lysophosphatidate- and thrombin-induced neurite retraction and neuronal cell rounding by ADP ribosylation of the small GTP-binding protein Rho. J. Cell Biol. *126*, 801–810.

Justice, R.W., Zilian, O., Woods, D.F., Noll, M., and Bryant, P.J. (1995). The *Drosophila* tumor suppressor gene *warts* encodes a homolog of human myotonic dystrophy kinase and is required for the control of cell shape and proliferation. Genes Dev. *9*, 534–546.

Katoh, H., Aoki, J., Ichikawa, A., and Negishi, M. (1998). p160 RhoA-binding kinase ROKα. induces neurite retraction. J. Biol. Chem. *273*, 2489–2492.

Komatsu, H., Mori, I., Rhee, J.-S., Akaike, N., and Ohshima, Y. (1996). Mutations in a cyclic nucleotide-gated channel lead to abnormal thermosensation and chemosensation in *C. elegans*. Neuron *17*, 707–718.

Kozma, R., Ahmed, S., Best, A., and Lim, L. (1995). The Ras-related protein Cdc42Hs and bradykinin promote formation of peripheral actin microspikes and filopodia in Swiss 3T3 fibroblasts. Mol. Cell. Biol. *15*, 1942–1952.

Leung, T., Chen, X.Q., Manser, E., and Lim, L. (1996). The p160 RhoA-binding kinase ROK alpha is a member of a kinase family and is involved in the reorganization of the cytoskeleton. Mol. Cell. Biol. *16*, 5313–5327.

Leung, T., Chen, X.Q., Tan, I., Manser, E., and Lim, L. (1998). Myotonic dystrophy kinase-related Cdc42-binding kinase acts as a Cdc42 effector in promoting cytoskeletal reorganization. Mol. Cell. Biol. *18*, 130–140.

Leung, T., Manser, E., Tan, L., and Lim, L. (1995). A novel serine/threonine kinase binding the Ras-related RhoA GTPase which translocates the kinase to peripheral membranes. J. Biol. Chem. *270*, 29051–29054.

Luo, L., Lee, T., Tsai, L., Tang, G., Jan, L.Y., and Jan, Y.N. (1997). Genghis Khan (Gek) as a putative effector for *Drosophila* Cdc42 and regulator of actin polymerization. Proc. Natl. Acad. Sci. USA *94*, 12963–12968.

Luo, L., Liao, Y.J., Jan, L.Y., and Jan, Y.N. (1994). Distinct morphogenetic functions of similar small GTPases: *Drosophila* Drac1 is involved in axonal outgrowth and myoblast fusion. Genes Dev. *8*, 1787–1802.

Madaule, P., Eda, M., Watanabe, N., Fujisawa, K., Matsuoka, T., Bito, H., Ishizaki, T., and Narumiya, S. (1998). Role of citron kinase as a target of the small GTPase Rho in cytokinesis. Nature *394*, 491–494.

Marcus, S., Polverino, A., Chang, E., Robbins, D., Cobb, M.H., and Wigler, M.H. (1995). Shk1, a homolog of the *Saccharomyces cerevisiae* Ste20 and mammalian p65PAK protein kinases, is a component of a Ras/Cdc42 signaling module in the fission yeast *Schizosaccharomyces pombe*. Proc. Natl. Acad. Sci. USA *92*, 6180–6184.

Matsui, T., Amano, M., Yamamoto, T., Chihara, K., Nakafuku, M., Ito, M., Nakano, T., Okawa, K., Iwamatsu, A., and Kaibuchi, K. (1996). Rho-associated kinase, a novel serine/threonine kinase, as a putative target for small GTP binding protein Rho. EMBO J. *15*, 2208–2216.

Mello, C.C., Kramer, J.M., Stinchcomb, D., and Ambros, V. (1991). Efficient gene transfer in *C. elegans*: extrachromosomal maintenance and integration of transforming sequences. EMBO J. *10*, 3959–3970.

Millward, T., Cron, P., and Hemmings, B.A. (1995). Molecular cloning and characterization of a conserved nuclear serine(threonine) protein kinase. Proc. Natl. Acad. Sci. USA *92*, 5022–5026.

Millward, T.A., Heizmann, C.W., Schafer, B.W., and Hemmings, B.A. (1998). Calcium regulation of Ndr protein kinase mediated by S100 calcium-binding proteins. EMBO J. *17*, 5913–5922.

Mohler, W.A., Simske, J.S., Williams-Masson, E.M., Hardin, J.D., and White, J.G. (1998). Dynamics and ultrastructure of developmental cell fusions in the *Caenorhabditis elegans* hypodermis. Curr. Biol. *24*, 1087–1090.

Mueller, B.K. (1999). Growth cone guidance: first steps towards a deeper understanding. Annu. Rev. Neurosci. *22*, 351–388.

Nobes, C.D., and Hall, A. (1995). Rho, Rac, and Cdc42 GTPases regulate the assembly of multimolecular focal complexes associated with actin stress fibers, lamellipodia, and filopodia. Cell *81*, 53–62.

Ottilie, S., Miller, P.J., Johnson, D.I., Creasy, C.L., Sells, M.A., Bagrodia, S., Forsburg, S.L., and Chernoff, J. (1995). Fission yeast *pak1+* encodes a protein kinase that interacts with Cdc42p and is involved in the control of cell polarity and mating. EMBO J. *14*, 5908–5919.

Paterson, H.F., Self, A.J., Garrett, M.D., Just, I., Aktories, K., and Hall, A. (1990). Microinjection of recombinant p21rho induces rapid changes in cell morphology. J. Cell Biol. *111*, 1001–1007.

Peckol, E.L., Zallen, J.A., Yarrow, J.C., and Bargmann, C.I. (1999). Sensory activity affects sensory axon development in *C. elegans*. Development *126*, 1891–1902.

Reiner, D.J., Newton, E.M., Tian, H., and Thomas, J.H. (1999). Diverse behavioral defects caused by mutations in *Caenorhabditis elegans unc-43* CaM kinase II. Nature *402*, 199–203.

Ridley, A.J., and Hall, A. (1992). The small GTP-binding protein Rho regulates the assembly of focal adhesions and actin stress fibers in response to growth factors. Cell *70*, 389–399.

Ridley, A.J., Paterson, H.F., Johnston, C.L., Diekmann, D., and Hall, A. (1992). The small GTP-binding protein Rac regulates growth factor-induced membrane ruffling. Cell *70*, 401–410.

Steven, R., Kubiseski, T.J., Zheng, H., Kulkarni, S., Mancillas, J., Ruiz Morales, A., Hogue, C.W., Pawson, T., and Culotti, J. (1998). UNC-73 activates the Rac GTPase and is required for cell and growth cone migrations in *C. elegans*. Cell *92*, 785–795.

St. John, M.A., Tao, W., Fei, X., Fukumoto, R., Carcangiu, M.L., Brownstein, D.G., Parlow, A.F., McGrath, J., and Xu, T. (1999). Mice deficient of Lats1 develop soft-tissue sarcomas, ovarian tumors and pituitary dysfunction. Nat. Genet. *21*, 182–186.

Tan, J.L., Ravid, S., and Spudich, J.A. (1992). Control of nonmuscle myosins by phosphorylation. Annu. Rev. Biochem. *61*, 721–759.

Tapon, N., and Hall, A. (1997). Rho, Rac, and Cdc42 GTPases regulate the organization of the actin cytoskeleton. Curr. Opin. Cell Biol. *9*, 86–92.

Tessier-Lavigne, M., and Goodman, C.S. (1996). The molecular biology of axon guidance. Science *274*, 1123–1133.

Verde, F., Mata, J., and Nurse, P. (1995). Fission yeast cell morphogenesis: identification of new genes and analysis of their role during the cell cycle. J. Cell Biol. *131*, 1529–1538.

Verde, F., Wiley, D.J., and Nurse, P. (1998). Fission yeast Orb6, a ser/thr protein kinase related to mammalian Rho-kinase and myotonic dystrophy kinase, is required for maintenance of cell polarity and coordinates cell morphogenesis with the cell cycle. Proc. Natl. Acad. Sci. USA *95*, 7526–7531.

Wang, F.S., Wolenski, J.S., Cheney, R.E., Mooseker, M.S., and Jay, D.G. (1996). Function of myosin-V in filopodial extension of neuronal growth cones. Science *273*, 660–663.

Wang, J., Renger, J.J., Griffith, L.C., Greenspan, R.J., and Wu, C.F. (1994). Concomitant alterations of physiological and developmental

plasticity in *Drosophila* CaM kinase II-inhibited synapses. Neuron *13*, 1373–1384.

Wang, K.H., Brose, K., Arnott, D., Kidd, T., Goodman, C.S., Henzel, W., and Tessier-Lavigne, M. (1999). Biochemical purification of a mammalian slit protein as a positive regulator of sensory axon elongation and branching. Cell *96*, 771–784.

Wissmann, A., Ingles, J., McGhee, J.D., and Mains, P.E. (1997). *Caenorhabditis elegans* LET-502 is related to Rho-binding kinases and human myotonic dystrophy kinase and interacts genetically with a homolog of the regulatory subunit of smooth muscle myosin phosphatase to affect cell shape. Genes Dev. *11*, 409–422.

Wu, G.Y., and Cline, H.T. (1998). Stabilization of dendritic arbor structure in vivo by CaMKII. Science *279*, 222–226.

Xu, T., Wang, W., Zhang, S., Stewart, R.A., and Yu, W. (1995). Identifying tumor suppressors in genetic mosaics: the *Drosophila lats* gene encodes a putative protein kinase. Development *121*, 1053–1063.

Yarden, O., Plamann, M., Ebbole, D.J., and Yanofsky, C. (1992). *cot-1*, a gene required for hyphal elongation in *Neurospora crassa*, encodes a protein kinase. EMBO J. *11*, 2159–2166.

Yu, S., Avery, L., Baude, E., and Garbers, D.L. (1997). Guanylyl cyclase expression in specific sensory neurons: a new family of chemosensory receptors. Proc. Natl. Acad. Sci. USA *94*, 3384–3387.

Zallen, J.A., Kirch, S.A., and Bargmann, C.I. (1999). Genes required for axon pathfinding and extension in the *C. elegans* nerve ring. Development *126*, 3679–3692.

Zipkin, I.D., Kindt, R.M., and Kenyon, C.J. (1997). Role of a new Rho family member in cell migration and axon guidance in *C. elegans*. Cell *90*, 883–894.

Zorio, D.A., Cheng, N.N., Blumenthal, T., and Spieth, J. (1994). Operons as a common form of chromosomal organization in *C. elegans*. Nature *372*, 270–272.